Many-Body Contact Repulsion of Deformable Disks

A. Šiber[1,2] and P. Ziherl[2,3]

[1]Institute of Physics, Bijenička cesta 46, 10000 Zagreb, Croatia
[2]Jožef Stefan Institute, Jamova 39, SI-1000 Ljubljana, Slovenia
[3]Faculty of Mathematics and Physics, University of Ljubljana, Jadranska 19, SI-1000 Ljubljana, Slovenia

(Received 7 January 2013; published 24 May 2013)

We use a spring-and-plaquette network model to analyze the repulsion between elastic disks in contact. By studying various 2D geometries, we find that as disks approach the incompressibility limit the many-body effects become dominant and the disk-disk interaction is not pairwise additive. Upon compression, the disks undergo a transition from the localized to the distributed deformation regime accompanied by a steep increase of energy consistent with the onset of a hard core. These results shed new light on the structures formed by deformable objects such as soft nanocolloids.

DOI: 10.1103/PhysRevLett.110.214301 PACS numbers: 46.25.−y, 61.50.Ah, 64.70.pv

Packing problems permeate the physics of colloids [1] and many aspects of regular and disordered colloidal structures can be interpreted by approximating the particles by hard spheres. Yet there exist colloidal systems marked by short-range repulsion which depart from the hard-sphere model. Notable examples include nanocolloidal materials based on microgels [2,3], star polymers [4], and self-assembled block copolymer [5–7] and dendrimer micelles [8,9]. Central for the understanding of soft colloids is the effective interaction between them [10] which may be derived theoretically [4] or from numerical simulations [11]. Although the concept of softness is by no means universal, all effective interactions in soft colloids (e.g., core-softened potentials [12–14], penetrable-sphere potentials [15,16], potentials given by a power of indentation [17]) reflect their deformability and penetrability in some way.

As a rule, effective interaction is pairwise additive and its choice is the key element in the hierarchy leading from the microscopic architecture of nanocolloids to the theoretical insight into their condensed phases. A popular model originating in the macroscopic contact mechanics is the Hertzian potential which has been used to describe the phase behavior of soft spheres [18,19], their jamming [17], and glassy dynamics [20], etc. But the deformation of elastic bodies is nonlocal and any interaction stemming from it is inherently not pairwise additive, which renders the notion of an effective pair potential in deformable nanocolloids questionable.

The aim of this Letter is to expose the role of many-body interactions between soft bodies in contact. We use a transparent mesoscopic model halfway between a coarse-grained representation of colloids where the nonpairwise character of the colloid-colloid forces is retained but not resolved [21], and an effective single-particle description. We focus on the deformation of colloids arranged on simple lattices so as to explore the effect of local confinement, and we quantify the magnitude of many-body interactions. Also studied is the validity of the Hertzian regime and the transition from localized to distributed deformations. Finally, we discuss the relevance of these results for structures formed by soft particles.

Our 2D model of a soft colloid or a nanocolloidal micelle is a disk of radius R excised from a triangular network of Hookean springs which subsume the covalent bonds within the particle as well as any entropic elasticity. Also included is the area elasticity of the triangular plaquettes formed by springs, which represents excluded-volume interactions; a similar framework was used to model polymer-chain networks [22,23]. The total spring-and-plaquette energy reads

$$E = \frac{k}{2}\sum_j (l_j - l_0)^2 + c_a \sum_J \left(1 - \frac{a_0}{a_J}\right)^2, \tag{1}$$

where k is the spring constant and c_a is the plaquette area-elasticity modulus; l_j is the spring length, a_J is the plaquette area, and l_0 and $a_0 = \sqrt{3}l_0^2/4$ are their equilibrium values, respectively; j runs over all springs and J runs over all plaquettes.

In the small deformation regime, this model can be related to bulk isotropic Hookean elasticity, its effective Young modulus Y and Poisson ratio ν being

$$Y = \frac{\sqrt{3}k}{2}(1 + \nu), \tag{2}$$

$$\nu = \frac{1}{2} - \frac{1}{4[1 + 16c_a/(3kl_0^2)]}, \tag{3}$$

where 3D relations between the Lamé moduli and Y and ν were used: $\lambda = \nu Y/[(1 + \nu)(1 - 2\nu)]$ and $\mu = Y/[2(1 + \nu)]$. The limit of $c_a = 0$ corresponds to the Poisson solid with $\nu = 1/4$. For $c_a \to \infty$, the network becomes incompressible and $\nu = 1/2$. As in most common materials ν ranges between 0.2 and 0.5, this model may be considered fairly general. With $R = 100l_0$ and a

total of 36 295 nodes, our disks are good approximation of an elastic continuum for strains larger than $l_0/R = 10^{-2}$.

To quantify the many-body effects, we compute the energy of the disk in the columnar, honeycomb, square, and hexagonal lattice where the disk is trapped between $n = 2$, 3, 4, and 6 symmetrically arranged neighbors, respectively (Fig. 1). On a lattice, balance of forces on a single disk is guaranteed by symmetry, ensuring that a bulk system can be represented by a unit cell. Our unit cells are regular n-gons such that the radius of the inscribed circle is $R - h$ where h is disk indentation; the only exception is the columnar lattice with a stripelike unit cell. The four lattices considered were chosen so as to emphasize the role of coordination number n, and generalization to other 2D lattices is straightforward.

We first look into the columnar lattice—a necklace of disks which is strictly speaking not globally stable. Figure 2 shows the energy of a disk in the columnar lattice as a function of relative indentation h/R for five different $c_a/(kl_0^2)$ corresponding to $\nu = 0.251$ $[c_a/(kl_0^2) = 10^{-3}]$, 0.263 (10^{-2}), 0.337 (10^{-1}), 0.461 (10^{0}), and 0.495 (10^{1}). The equilibrium disk shape was obtained by minimizing the energy using conjugate gradient method [24] and constraints were enforced by energy penalization [25]. During relaxation, the network did not undergo any refinement and its topology was unchanged.

One observes an important difference between disks of Poisson ratio close to 1/4 and 1/2. For $\nu \approx 1/4$, the Hertzian-like dependence of energy $E \approx 1.088kR^2/(1-\nu)(h/R)^{2.2}$ [26] holds in a broad range of indentations (solid line in Fig. 2), whereas for $\nu \to 1/2$ the energy at large indentations is much bigger than the Hertzian prediction. This departure is mostly due to the significant overlap of the two indented regions close to the contact lines, which takes place for sufficiently large values of $c_a/(kl_0^2)$ and h/R [27]. As the deformation pattern is not a simple superposition of the two partial strains, the elastic energy includes many-body terms. The diverging energy of nearly incompressible disks of $c_a/(kl_0^2) \gg 1$ at $h/R \to 1$ can be approximated analytically by assuming that all plaquettes undergo uniform compression along the column and adjusting the transverse dilation so as to preserve the area. This gives

$$\lim_{\substack{\nu\to 1/2\\ h/R\to 1}} \frac{E}{kR^2} \approx \frac{\pi}{2\sqrt{3}} \frac{1 - 4h/R + 6(h/R)^2}{(1 - h/R)^2}, \tag{4}$$

which nicely agrees with the numerical results (dashed line in Fig. 2). Very similar behavior has been observed experimentally in polyacrylamide hydrogel spheres [28].

Data in Fig. 2 terminate at a point where the disk in a columnar lattice undergoes a partial plaquette collapse related to that seen in spring-only networks. At sufficiently large indentations and ν close to 1/4, the spring-and-plaquette network is characterized by striations and is similar to the two-phase regime of Ref. [23]. Disks in the other three lattices experience a more diverse variety of instabilities. As these modes are not our main interest, they were not pursued further and all results discussed here correspond to the network prior to any creasing, wrinkling, or striation transition.

We now compare the four lattices by computing the energy per neighbor

$$E_n = \frac{E}{n}. \tag{5}$$

For pairwise interactions, E_n does not depend on the coordination number n so that any variation observed is a signature of many-body effects. Figure 3 shows E_n for $c_a/(kl_0^2) = 10^{-3}$ and 10^1 corresponding to $\nu = 0.251$ and 0.495, respectively. The noncoinciding energies per neighbor in Fig. 3(a) demonstrate that many-body effects are present even if the area term is small $[c_a/(kl_0^2) = 10^{-3}$, Fig. 3(a)]. Yet their importance does not depend much on indentation: At $h/R = 0.02$, E_6 amounts to 123% of E_2,

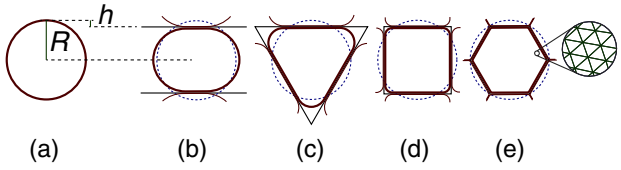

FIG. 1 (color online). Columnar (b), honeycomb (c), square (d), and hexagonal (e) lattice. Thin lines represent the unit cells—stripe, equilateral triangle, square, and regular hexagon, respectively—at identical indentations h. Thick lines illustrate the contours of deformed disks (partly shown are their neighbors), and panel (a) and dashed circles are undeformed disks of radius R drawn for comparison. Also included is a schematic of the spring-and-plaquette network.

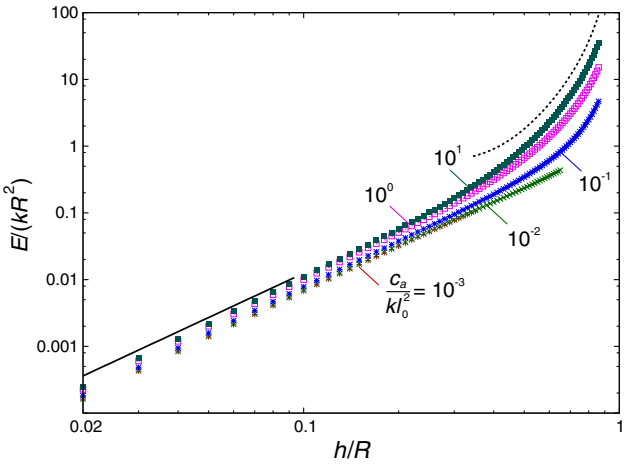

FIG. 2 (color online). Reduced energy of a disk in columnar lattice vs relative indentation for five different values of $c_a/(kl_0^2)$. The solid line shows the Hertzian energy $E \propto (h/R)^{2.2}$ and the dashed line is the variational prediction for incompressible deformation [Eq. (4)].

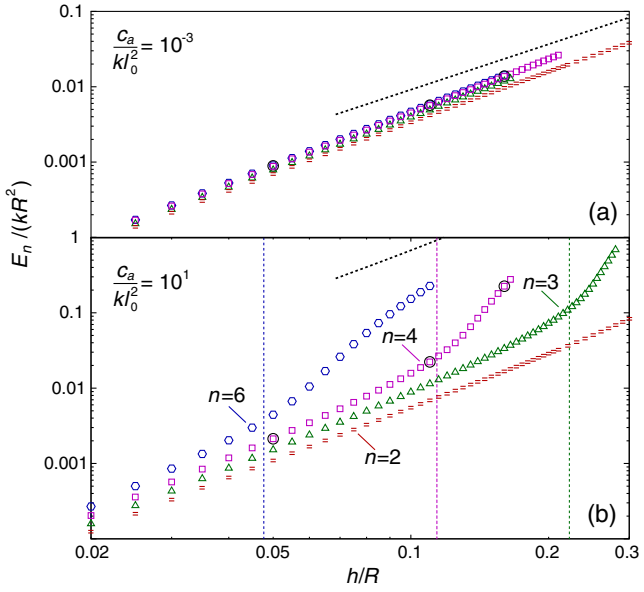

FIG. 3 (color online). Energy per neighbor E_n in an almost Poisson-solid disk $[c_a/(kl_0^2) = 10^{-3}$; panel (a)] and in an almost incompressible disk $[c_a/(kl_0^2) = 10^{1}$; panel (b)] in columnar, honeycomb, square, and hexagonal lattice vs relative indentation. The data for each lattice are represented by a symbol in the shape of the unit cell. The black dashed line shows $1/6$ of the energy of an isotropically compressed disk. The meaning of the vertical dashed lines and open circles is explained in the text.

whereas at $h/R = 0.2$ $E_6/E_2 = 145\%$. We see that E_n is an increasing function of n for all h/R. This is expected—a large coordination number means that the indented regions are close to each other, which gives rise to pronounced many-body effects. Also shown is $1/6$ of the energy of an isotropically compressed disk such that the relative decrease of its radius is h/R. This energy indicates the general trend of E_3, E_4, and E_6 at large h/R and it serves as a rough upper analytical estimate of E_6, the most isotropic of all lattices.

In nearly incompressible disks E_n are clearly separated $[c_a/(kl_0^2) = 10^{1}$; Fig. 3(b)], showing that the many-body effects are very strong and that they increase with the coordination number. Furthermore, in each $E_{n>2}$ a steep energy increase is observed at a certain threshold indentation $(h/R)_t$ beyond which area-preserving deformation is no longer geometrically possible. At the threshold the unit cell area is equal to the area of undeformed disk, yielding $(h/R)_t = 0.222$, 0.114, and 0.048 for honeycomb, square, and hexagonal lattice, respectively. These values are plotted by vertical dashed lines in Fig. 3(b).

The steep post-threshold energy increase at large $c_a/(kl_0^2)$ can be interpreted as the onset of a "hard-core" interaction in the sense that in this regime, deformations caused by contacts with neighbors propagate throughout the disk. The difference between the soft regime at small h/R and the hard post-threshold regime is illustrated by Fig. 4(b) which shows the distribution of energy density in a nearly incompressible disk with $c_a/(kl_0^2) = 10^{1}$ in the square lattice for three indentations [encircled symbols in Fig. 3(b)]. For small indentations $(h/R = 0.05)$, the deformations are localized in subsurface regions close to contact lines and the disk core is stress-free. In this regime the energy is pairwise additive to a good approximation, although the faint diamondlike pattern connecting the indented regions signals many-body effects. At the threshold $(h/R = 0.11)$ deformation is still localized but the

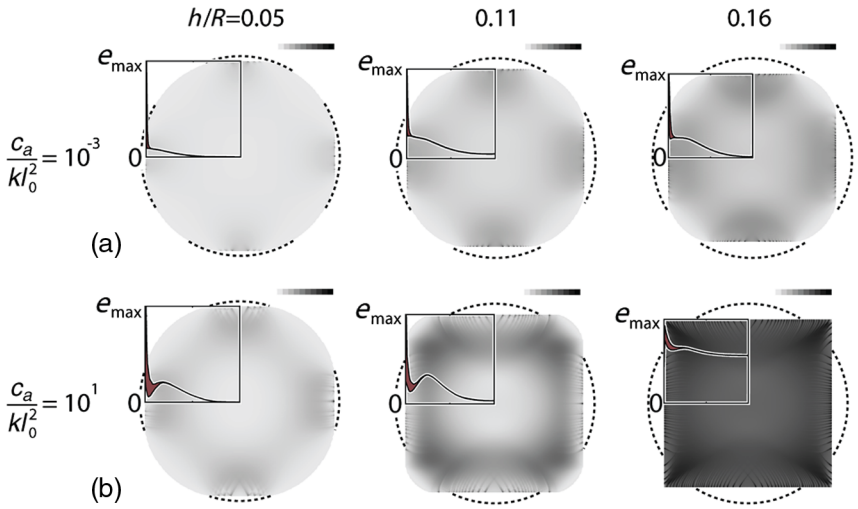

FIG. 4 (color online). Distribution of energy density in compressible $[c_a/(kl_0^2) = 10^{-3}$; panel (a)] and nearly incompressible disks $[c_a/(kl_0^2) = 10^{1}$; panel (b)] in the square lattice for three different relative indentations $h/R = 0.05$, 0.11, and 0.16. The energy density is color-coded such that the lightest shade of gray represents zero whereas black corresponds to maximal energy density e_{max}, which is different in each panel. The insets show the energy density profiles at the horizontal midline. To accommodate the variations caused by the discreteness of the network, we plotted all profiles within a narrow interval of width $0.04(R - h)$ around the midline, hence the spread of the curves immediately underneath the contact line.

overlap of indented regions is significant so that they form a connected domain around an almost undeformed core. Beyond the threshold ($h/R = 0.16$) the energy density profile is changed dramatically and the deformation is fairly uniform. For comparison, we also show the energy density distribution in a compressible disk with $c_a/(kl_0^2) = 10^{-3}$ [Fig. 4(a)]. Here, the situation is quite different and the quasi-Hertzian regime with weakly coupled subsurface deformations and a stress-free core persists at all h/R examined.

From the analysis of interaction energies [Fig. 3(b)] and energy distribution patterns (Fig. 4) emerges the notion of the *disk core* as a physical object characteristic of nearly incompressible disks. The core is the central part of the disk that is unstressed in the pre-threshold quasi-Hertzian regime whereas beyond the threshold it undergoes a virtually uniform deformation, transmitting stresses across the disk. The transition is accompanied by a steep increase of energy reminiscent of true hard-core repulsion, which allows us to introduce the core on both energetic and geometric grounds. Moreover, this behavior suggests that deformable but nearly incompressible disks can be referred to as *semihard* because they share the features of hard (undeformable and incompressible) and soft (deformable and compressible) particles.

The transition from quasi-Hertzian to stressed-core regime in nearly incompressible disks, which depends on the number of neighbors, may be approximated by a coordination-dependent effective interaction. Although such a concept would strictly apply only to regular local configurations, the outcome could be quite interesting. Consider a horizontal cut across Fig. 3(b) corresponding to a certain thermal energy, which shows that at a given temperature the maximal indentation defined by $E_n(h_{\max}/R) \sim k_BT$ depends on n. For $k_BT \lesssim 0.001kR^2$ the apparent hard-core diameter $R - h_{\max}$ of a six-coordinated disk is only about 1% larger than that of a two-coordinated disk, which is negligible. But for $k_BT \approx 0.1kR^2$ the spread of apparent hard-core diameters reaches $\approx 20\%$ making two-coordinated disks behave as if they were much smaller than six-coordinated ones. At high enough temperatures and intermediate densities, a suspension of nearly incompressible disks may be characterized by an effective dynamic polydispersity in terms of disks' apparent size and pair interactions, rendering it somewhat similar to polydisperse colloids [29].

In conclusion, the two examples presented in Fig. 3 show that interaction between elastic particles depends very much on their compressibility. As this behavior is specific neither to two dimensions nor to the regular local configurations explored here, they should apply equally to 3D elastic bodies in both crystalline and disordered structures, leading to several interesting conclusions and phenomena. First, our results show that the Hertzian approximation is reasonable in particles of moderate Poisson ratio where the many-body effects are limited, suggesting that the complex theoretical phase diagrams of Hertzian spheres [18,19] describe well the behavior of such particles at intermediate densities. Second, the nearly incompressible-particle regime may well serve as a model for microgel spheres. The Poisson ratio of a single sphere can be measured using the capillary micromechanics technique and in pNIPAM particles it is about 0.42 [30], which puts them close to the incompressible limit of $\nu = 1/2$. The phase behavior of microgels was shown to differ from that of hard spheres, one of the main deviations being a larger effective packing fraction at melting [2]. This effect could be related to the dynamic size polydispersity experienced by disordered particles, which should conceivably enhance the stability of the fluid phase. Third, the nonfragile glassy behavior of dense microgel suspensions [31] has been tentatively explained in terms of the directionality of interparticle interactions caused by faceting upon compression. Absent in hard spheres and limited in compressible particles [Fig. 4(a)], faceting is very prominent in nearly incompressible particles. Our predictions provide a qualitative microscopic basis of these phenomena, and they call for a comprehensive analysis of contact mechanics of 3D soft and semihard spheres.

We acknowledge discussions with L. Athanasopoulou and G. Skačej. This work was supported by the Marie-Curie Initial Training Network COMPLOIDS (FP7-PEOPLE-ITN-2008 Grant No. 234810), by the Ministry of Science, Education, and Sports of the Republic of Croatia (Grant No. 035-0352828-2837), and by the Slovenian Research Agency (Grant No. P1-0055).

[1] T. Aste and D. Weaire, *The Pursuit of Perfect Packing* (Institute of Physics Publishing, London, 2000).
[2] H. Senff and W. Richtering, J. Chem. Phys. **111**, 1705 (1999).
[3] M. Ballauff and Y. Lu, Polymer **48**, 1815 (2007).
[4] C. N. Likos, H. Löwen, M. Watzlawek, B. Abbas, O. Jucknischke, J. Allgaier, and D. Richter, Phys. Rev. Lett. **80**, 4450 (1998).
[5] T. P. Lodge, B. Pudil, and K. J. Hanley, Macromolecules **35**, 4707 (2002).
[6] G. A. McConnell, A. P. Gast, J. S. Huang, and S. D. Smith, Phys. Rev. Lett. **71**, 2102 (1993).
[7] G. Riess, Prog. Polym. Sci. **28**, 1107 (2003).
[8] V. S. K. Balagurusamy, G. Ungar, V. Percec, and G. Johansson, J. Am. Chem. Soc. **119**, 1539 (1997).
[9] X. Zeng, G. Ungar, Y. Liu, V. Percec, A. E. Dulcey, and J. K. Hobbs, Nature (London) **428**, 157 (2004).
[10] C. N. Likos, Phys. Rep. **348**, 267 (2001).
[11] B. M. Mladek, G. Kahl, and C. N. Likos, Phys. Rev. Lett. **100**, 028301 (2008).
[12] D. A. Young and B. J. Alder, Phys. Rev. Lett. **38**, 1213 (1977).
[13] E. A. Jagla, Phys. Rev. E **58**, 1478 (1998).

[14] E. Velasco, L. Mederos, G. Navascués, P. C. Hemmer, and G. Stell, Phys. Rev. Lett. **85**, 122 (2000).
[15] A. A. Louis, P. G. Bolhuis, J. P. Hansen, and E. J. Meijer, Phys. Rev. Lett. **85**, 2522 (2000).
[16] B. M. Mladek, D. Gottwald, G. Kahl, M. Neumann, and C. N. Likos, Phys. Rev. Lett. **96**, 045701 (2006).
[17] M. van Hecke, J. Phys. Condens. Matter **22**, 033101 (2010).
[18] J. C. Pàmies, A. Cacciuto, and D. Frenkel, J. Chem. Phys. **131**, 044514 (2009); **131**, 159903 (2009).
[19] S. Prestipino, F. Saija, and G. Malescio, Soft Matter **5**, 2795 (2009).
[20] L. Berthier, A. J. Moreno, and G. Szamel, Phys. Rev. E **82**, 060501(R) (2010).
[21] C. R. Iacovella, A. S. Keys, and S. C. Glotzer, Proc. Natl. Acad. Sci. U.S.A. **108**, 20 935 (2011).
[22] S. K. Boey, D. H. Boal, and D. E. Discher, Biophys. J. **75**, 1573 (1998).
[23] W. Wintz, R. Everaers, and U. Seifert, J. Phys. I **7**, 1097 (1997).
[24] W. W. Hager and H. Zhang, SIAM J. Optim. **16**, 170 (2005).
[25] A. Šiber, Phys. Rev. E **73**, 061915 (2006).
[26] K. L. Johnson, *Contact Mechanics* (Cambridge University Press, Cambridge, England, 1985).
[27] To a small extent, the deviation is caused by the inapplicability of Hertzian prediction at large indentations.
[28] S. Mukhopadhyay and J. Peixinho, Phys. Rev. E **84**, 011302 (2011).
[29] P. Sollich, J. Phys. Condens. Matter **14**, R79 (2002).
[30] M. Guo and H. M. Wyss, Macromol. Mater. Eng. **296**, 223 (2011).
[31] J. Mattsson, H. M. Wyss, A. Fernandez-Nieves, K. Miyazaki, Z. Hu, D. R. Reichman, and D. A. Weitz, Nature (London) **462**, 83 (2009).